Parameter estimation using multifrequency range-dependent acoustic data in shallow water

Peter Gerstoft and Donald F. Gingras
SACLANT Undersea Research Centre, 19138 La Spezia, Italy

(Received 1 June 1995; accepted for publication 29 January 1996)

The estimation of all forward model parameters—geometric, geoacoustic, and ocean sound speed—by the inversion of acoustic field observations is considered. The data was taken at a mildly range-dependent shallow water site in the Mediterranean Sea. The inversion is based on data from a vertical array and carried out using information at multiple frequencies. Global optimization using a directed Monte Carlo search based on genetic algorithms and the Bartlett objective function is used. All geometric parameters are well determined, a range-dependent geoacoustic model is determined, and the ocean sound speed is estimated. Comparisons of the observed pressure field as a function of depth and the predicted field show good agreement. The use of observations at multiple frequencies provides considerable stability for the estimated parameters. Optimization of only geometric and geoacoustic parameters in a range-independent environment is found to be satisfactory at the lower frequencies (165–175 Hz), but for the higher frequencies (325–335 Hz) optimization of additional parameters by inclusion of either a range-dependent forward model or the ocean-sound-speed profile seems essential for successful inversion.

PACS numbers: 43.30.Wi, 43.60.Pt

INTRODUCTION

In October 1993 SACLANTCEN conducted an experiment in the Mediterranean Sea using a moored source and vertical array in shallow water. An objective of the experiment was to evaluate the performance of field inversion methods in shallow water under somewhat optimal conditions, i.e., an array that spanned most of the water column, knowledge of hydrophone positions via active array positioning, and a fixed geometry for source and receivers. In an earlier paper, see Ref. 1, these data were used to establish the stability with respect to time of environmental parameter estimates using a range-independent model at a single frequency (169.9 Hz). During the experiment two signal bands were used, a band centered at 170 Hz and a band centered at 335 Hz. The emphasis of this paper is on the use of multifrequency data from both bands for the estimation of the geometric, geoacoustic, and ocean sound-speed parameters using a global optimization approach. Using the combined frequency data it was expected that the low-frequency data would provide estimates for the large scale features, whereas the higher frequency data would provide finer scale details about the parameters. The inversion process for determining environmental parameters is, in principle, straightforward. In theory it requires determining the forward model parameters that accurately match the observed data. The methods are based on global optimization for a selected objective function. The optimization procedures are now quite efficient and are based on simulated annealing[2–4] genetic algorithms[5] or a combination of these and a local method.[6] Herein the SAGA code[7] which uses genetic algorithms for optimization was used.

Three important issues associated with the inversion of field data for parameter estimation are the data domain (time versus frequency and/or narrow band versus broadband), the forward model (range dependent or range independent), and the inclusion of additional environmental parameters such as ocean sound speed. Matched-field processing has typically been carried out in the frequency domain using only one frequency cell. Recently, there has been increased interest in multifrequency approaches.[8–14] A multifrequency approach has been adopted herein for the estimation of all environmental parameters. Often for inversion purposes a range-independent environment is sufficient, but range-dependent models based on the parabolic equation[2] or adiabatic modes[4] have been considered. The adiabatic mode approach was used with modal look-up tables; this makes the approach quite fast. However, when many parameters of different dimension are considered the construction of the tables could become a considerable task. The SAGA program uses range-dependent adiabatic modes directly. Most inversion work reported previously has only considered estimation of the geoacoustic parameters. For matched-field processing it has been well established that even small fluctuations in ocean sound-speed can cause a major degradation, see, e.g., Refs. 15–17. Therefore, it seems natural to include sound-speed estimation as part of the optimization, and this issue is investigated here.

In this paper, global estimation methods based on genetic algorithms (GA) were applied to experimental data. With respect to most previous work three issues were extended: (i) observations from multiple frequencies were used, (ii) a range-dependent forward model was employed, and (iii) all important forward model parameters, including ocean sound-speed, were used in the optimization. In Sec. I the multifrequency objective function is introduced along with details about the inversion process. The ocean sound-speed estimation methods are also presented. In Sec. II a brief description of the experimental setup is discussed and

the ''baseline'' environmental model is presented. In Sec. III estimation results based on synthetic data for the baseline environment are presented. In Sec. IV results of multifrequency inversion of experimental data using both a range-independent and a range-dependent model are presented along with the results obtained for ocean sound-speed estimation. Finally, in Sec. V the conclusions are presented.

Throughout, the following terminology will be used; an ''environmental model'' will consist of all geometric, geoacoustic, and ocean sound-speed parameters required for the forward propagation model. The following notation is used throughout; boldface upper case letters denote matrices, boldface lower case letters denote column vectors, $\mathbf{u}^T$ denotes vector transpose, $\mathbf{u}^c$ denotes complex conjugate, and $\mathbf{u}^*$ denotes complex conjugate transpose.

I. PRELIMINARIES

The components of the acoustic inversion process include an environmental model, a propagation model for calculating the predicted acoustic field, an objective function, a model vector $\mathbf{m}=\{m_i\}$ $i=1,2,\ldots,N$, and an efficient search algorithm for searching the model parameter space. The objective function is a function of a vector of forward model predictions or replica $\mathbf{w}(\mathbf{m})$ fields and a vector of observations $\mathbf{q}=\{q_i\}$ $i=1,2,\ldots,K$, where K is the number of hydrophones. For the optimization genetic algorithms (GA) are used. The environmental model consists of three layers; a water layer, a fluid sediment layer and a homogeneous half-space layer. The inverse problem is solved as an optimization problem; that is, find the model vector $\mathbf{m}=\{m_i\}$ $i=1,2,\ldots,N$ that maximizes the objective function.

A. Objective function

In an earlier paper the Bartlett processor at a single frequency was used.[1] In order to improve the robustness of the estimation, observations at several frequencies were used in this analysis. Due to the CPU time involved only a few frequencies were used in the optimization. For L independent observations of the complex pressure across the array at frequencies ω_l, $l=1,\ldots,L$ an estimator was obtained by incoherently summing the values of the Bartlett processor at each frequency.[8] The resulting objective function is given by

$$\Phi(\mathbf{m})=\frac{1}{L}\sum_{l=1}^{L}\mathbf{w}^*(\mathbf{m},\omega_l)\hat{\mathbf{R}}(\omega_l)\mathbf{w}(\mathbf{m},\omega_l), \tag{1}$$

where $\hat{\mathbf{R}}(\omega_l)$ is the cross-spectral matrix formed from the observation vectors at a single frequency ω_l and $\mathbf{w}(\mathbf{m},\omega_l)$ is the replica vector calculated by the forward model. The matrix $\hat{\mathbf{R}}(\omega_l)$ is normalized such that the maximum Bartlett power is one. If the source spectrum is known then the summation in Eq. (1) could be weighted by the source spectrum [see for example, Ref. 18, Eq. (24)]. Herein the source spectrum was not known, thus a weighting of one was used for all frequencies. The following advantages resulting from an optimization over several frequencies are expected: (i) the variance of the estimates due to noise in the data becomes lower, (ii) the resulting estimates are valid over a range of frequencies—at least near the frequencies used in the inversion—and (iii) the low-frequency data can be used to focus the high-frequency data toward the optimum solution.

B. *Posteriori* analysis

For maximizing the objective function, Eq. (1), genetic algorithms (GA) were used.[5] During the optimization, all obtained samples of the search space were stored and used to estimate the *a posteriori* probabilities. For a system of M parameters the result is an M-dimensional space. This is difficult to display and only the marginal probability distributions are shown. The samples were ordered according to their energy and the probability distribution is scaled using a Boltzmann distribution.[5] Thus the objective function for each model vector is scaled according to a ''temperature'' T. The probability for the kth model vector is given by

$$\sigma(\mathbf{m}^k)=\frac{\exp[-(1-\Phi(\mathbf{m}^k))/T]}{\sum_{l=1}^{N_{\text{obs}}}\exp[-(1-\Phi(\mathbf{m}^l))/T]}, \tag{2}$$

where N_{obs} is the number of sampled model vectors. It is difficult to chose the value of the temperature: selecting it equal to the fittest sample favors the fittest part of the samples, whereas selecting it equal to the least fit penalizes the best fit. A good choice, shown by experience, is to use a temperature equal to the average of the best 50 samples.

For the ith parameter in the model vector the marginal probability distribution for obtaining the particular value κ can be found by summing Eq. (2):

$$\sigma_i(m_i=\kappa)=\frac{\sum_{k=1}^{N_{\text{obs}}}\exp[-(1-\Phi(\mathbf{m}^k))/T]\,\delta(m_i^k=\kappa)}{\sum_{k=1}^{N_{\text{obs}}}\exp[-(1-\Phi(\mathbf{m}^k))/T]}. \tag{3}$$

Based on the *a posteriori* probability distributions two estimates for the model parameters were used: Those with the largest fitness (GA-best), and those based on the mean of the *a posteriori* distribution (GA-mean). In the previous paper,[1] the GA-mean was used for the parameter estimate. The mean provided a good estimate for some frequencies and parametrizations, but at the higher frequencies it gave less reliable estimates. This was probably due to the fact that there were more peaks in the *a posteriori* distribution at the higher frequencies. When there is a few distinct peaks in the distribution, the mean value may not be a good estimate for the parameter, but the best value will be a good estimate. For these cases the GA-best gave more consistent results.

Based on the *a posteriori* distribution we can estimate the variance of each parameter. This variance consists of three separate parts: (1) variance due to noise in the data, (2) variance due to incorrect forward modeling, and (3) variance due to a poorly resolved parameter during the inversion. When using several frequencies the variance due to noise is expected to decrease, but the other contributions to the variance could increase.

The approach of hypothesis testing should ideally be used to judge if a more complex set of environmental parameters is better than a simpler set of parameters. Hypothesis testing has been used for the source localization problem, see, e.g., Ref. 19. As hypothesis testing is not available for testing sets of environmental parameters we had to rely on a

''satisfactory'' improvement in Bartlett power combined with the requirement that the environmental parameters were physically realistic. An indication that the additional parameters were important was obtained both from the increase in Bartlett power between the two inversions or the compactness of the *a posteriori* probability distribution for the additional parameters using just one inversion.

Insight into the estimation performance can be gained by comparing the Bartlett power across the array with the observed pressure (magnitude-squared) across the array. This is similar to the transmission loss data comparisons with model predictions that are used to illustrate estimation performance when the observations are a function of range, see for example Ref. 20. In order to obtain the Bartlett power across the array as described below the observed pressure vector $\mathbf{q}$ is required.

For a single frequency the Bartlett power can be expressed in terms of the pressures at the K hydrophones:

$$\Phi = (\mathbf{w}^*\mathbf{q})(\mathbf{w}^*\mathbf{q})^c = \sum_{k=1}^{K} w_k^c q_k (\mathbf{w}^*\mathbf{q})^c = \sum_{k=1}^{K} P_k(\mathbf{q},\mathbf{w}), \quad (4)$$

where

$$P_k(\mathbf{q},\mathbf{w}) = \mathrm{Real}[w_k^c q_k (\mathbf{w}^*\mathbf{q})^c]. \quad (5)$$

By taking the real part inside the sum in Eq. (4) a real expression for the Bartlett power contribution at each hydrophone was obtained, Eq. (5). It is seen that Eq. (5) contains cross terms with the other hydrophones. This is necessary in order to obtain a real expression that sums to the Bartlett power. Equation (5) is referred to as the Bartlett power measure. The maximum Bartlett power, one, is obtained when the replica corresponds to the data:

$$P_k(\mathbf{q},\mathbf{q}) = \mathrm{Real}[q_k^c q_k (\mathbf{q}^*\mathbf{q})^c] = q_k^c q_k . \quad (6)$$

The function $P_k(\mathbf{q},\mathbf{q})$ corresponds to the magnitude squared of the pressure for each hydrophone on the array. This measure represents the phase difference between the data and replica at each phone weighted with the corresponding amplitudes. Using, for example, the magnitude squared of the complex residuals as a measure is not very attractive as it requires knowledge of the absolute phase. By plotting the Bartlett power measure over the array, Eq. (5), as well as the magnitude-squared pressure, Eq. (6), a visual assessment of how well the estimated model prediction of the pressure across the array compares with the observed pressure is obtained.

C. Ocean sound-speed estimation

The estimation of ocean sound-speed profiles via acoustic tomography has received considerable attention, see for example Refs. 21, 22, 23. In general a sound-speed profile contains a large number of data points, thus optimization of the sound-speed profile directly could be cumbersome. This direct estimation of sound-speed points is the simplest approach as it directly reflects the parameters required for the forward modeling. The disadvantage is that this approach gives the optimization too much flexibility relative to the information available.

A more efficient representation is to describe the sound-speed via shape functions.[6] These can be seen as a coordinate transformation between the sound-speed vector $\mathbf{c}$ and a more efficient set of parameters μ_j:

$$\mathbf{c} = \sum_{j=1}^{J} \mu_j \mathbf{v}_j , \quad (7)$$

where $\mathbf{v}_j$ is the jth shape or basis function, μ_j is the coefficient associated with this shape function, and J is the number of shape functions, see the Appendix for additional detail.

For determining the ocean sound-speed via shape functions two methods were used: an ''*ad-hoc*'' method and a method based on empirical orthonormal functions (EOF),[24] see also the Appendix. The *ad-hoc* method is based on essential physics, i.e., detailed modeling of the thermocline and less detail for the upper and lower parts of the sound-speed profile. The sound speed in the sediment has also been modeled using this approach, see Secs. III and IV. The EOF method is based on actual measured sound-speed profiles. When sound-speed profile measurements are available it seems reasonable to use EOFs, but if measurements are not available then the *ad-hoc* method could be used.

II. NORTH ELBA ENVIRONMENT

This section contains a brief description of the experimental setup and details about the received signal structure as a function of frequency and depth. Also, the ''baseline'' environmental model constructed for the North Elba site is presented.

A. Experimental setup

The experimental data were collected over a two-day period on 26 and 27 October 1993 in a shallow water area north of the island of Elba, off the Italian west coast, where environmental conditions were known from earlier SACLANTCEN experiments.[25–27] This area is characterized by a flat bottom covered with clay and sand–clay sediments. The experiment was conducted in a flat area between the 120- and 140-m depth contours along a track running parallel to the depth contours. The propagation conditions were typical downward refracting summer conditions. Acoustic field data from the vertical array, array positioning data, ocean sound-speed profile and current versus depth profile data were acquired over the two-day period. For additional details on the North Elba site and experimental setup, see Ref. 1.

The bathymetry was measured to be approximately 128 m at the array site. The vertical array contained 48 hydrophones at 2-m spacing with a total aperture of 94 m. Based on the physical configuration of the array system and the measured bathymetry of 128 m at the array site the bottom hydrophone was at a depth of 112.7 m and the top hydrophone at a depth of 18.7 m. In order to determine the variation of the array hydrophone positions in the water column due to current an acoustic array positioning system was deployed with the vertical array. Estimates of array shape were computed over the two-day period. During the time period

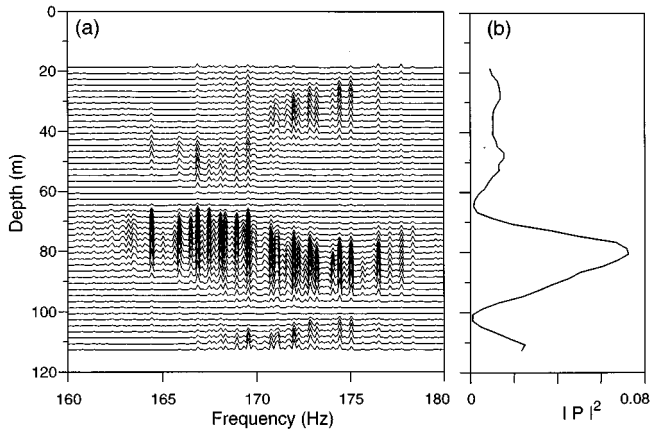

FIG. 1. The 170-Hz PRN signal as received on the vertical array; (a) power spectrum versus hydrophone depth and (b) magnitude squared of the pressure versus depth at 169.2 Hz.

that this data was collected the top of the array was displaced about 0.7 m from vertical. A detailed description of the array positioning system is available in Ref. 28.

A stationary source was deployed at a depth of 80 m and approximately 5600-m due north of the vertical array. At the source location the bathymetry was measured to be 130 m. Two signals were transmitted by the stationary source, both were continuous transmissions of pseudorandom noise (PRN) produced using a maximal length sequence. The first signal used a bit length of 52.9-ms modulated onto a carrier with center frequency of 170 Hz. The repetition length for this sequence was 3.1 s, and the −3-dB bandwidth was 12 Hz. The second signal used a bit length of 20 ms modulated to a center frequency of 335 Hz, the repetition length was 1.3 s, and the −3-dB bandwidth of 30 Hz.

Figure 1(a) illustrates an example of the 170-Hz signal power spectrum as a function of depth across the array aperture. Note the discrete ''pickets'' in frequency which are characteristic of the spectrum of PRN signals. Note also the variability of the received signal as a function of depth and as a function of frequency. Figure 2(a) illustrates the received signal spectrum for the signal centered at 335 Hz as a

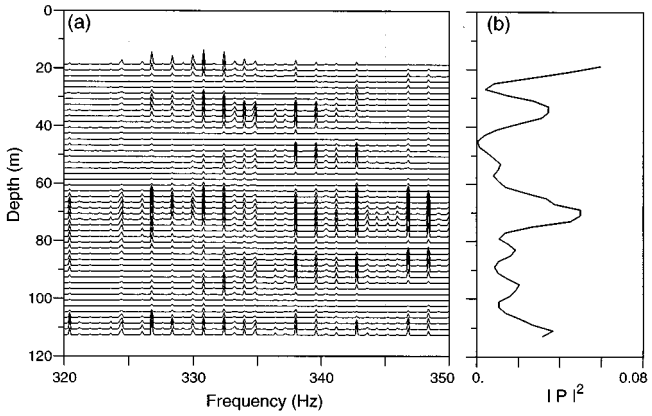

FIG. 2. The 335-Hz PRN signal as received on the vertical array; (a) power spectrum versus hydrophone depth and (b) magnitude squared of the pressure versus depth at 330.1 Hz.

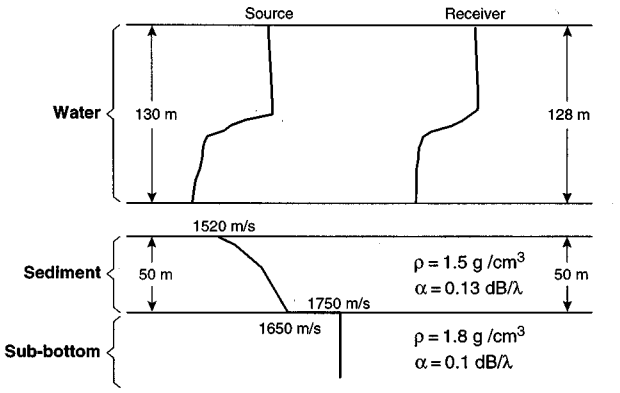

FIG. 3. The ''baseline'' environmental model based on measured ocean sound-speed profiles at the source and receiver, source and receiver bathymetry and published geoacoustic parameters for the North Elba experiment site, see also Table V.

function of depth. For this signal, since the repetition length is shorter, the ''pickets'' are spaced further apart in frequency. The pressure distribution as a function of depth at 330.1 Hz, see Fig. 2(b), is considerably more complicated than that at 169.2 Hz, see Fig. 1(b). This additional complexity can be explained by the fact that there are approximately twice as many modes propagating at 330.1 Hz versus 169.2 Hz.

B. The baseline environmental model

A baseline environmental model was established for the North Elba site from a variety of sources. The primary sources were the publications of Jensen[25] and Akal.[26,27] The results reported by Jensen and Akal were augmented by physical measurements taken during the experiment and by the results of Ref. 1. In addition the results of a recent sediment survey were included.[29] Figure 3 illustrates the range-dependent baseline environmental model. A range-dependent water layer overlying a constant thickness sediment layer

TABLE I. The range-dependent ''baseline'' environmental model.

Model parameter	Value
Geometric	
Source range (m)	5600
Source depth (m)	80
Receiver depth (m)	112.7
Array tilt (m)	0
Bathymetry-src (m)	130
Bathymetry-rcv (m)	128
Sediment	
Comp. speed, c_0 (m/s)	1520
Comp. speed, c_5 (m/s)	1550
Comp. speed, c_{20} (m/s)	1600
Comp. speed, c_{50} (m/s)	1650
Density (g/cm^3)	1.5
Attenuation (dB/λ)	0.13
Thickness (m)	50
Bottom	
Comp. speed, c_b (m/s)	1750
Density (g/cm^3)	1.8
Attenuation (dB/λ)	0.1

TABLE II. GA inversion model with parameter search bounds. Each parameter was discretized into 128 values.

Model parameter	Lower bound	Upper bound
Geometric		
Source range (m)	5300	5900
Source depth (m)	72	82
Array tilt (m)	−3	3
Receiver depth (m)	110	115
Bathymetry-src (m)	127	134
Bathymetry-rcv (m)	127	134
Sediment		
Sound speed, c_0 (m/s)	1510	1560
Sound speed, δ_1 (m/s)	0	100
Sound speed, δ_2 (m/s)	0	100
Sound speed, δ_3 (m/s)	0	100
Attenuation (dB/λ)	0	0.4
Bottom		
Sound speed, δ_4 (m/s)	0	200

with depth dependent sound-speed, and subbottom half-space layer. The source and receiver sound-speed profiles were based on a CTD taken near the vertical array and the source buoy, respectively. The important differences between this baseline model and that used previously in Ref. 1 are sediment thickness, the use of two sound-speed profiles, two bathymetry measurements and the addition of array tilt. The baseline value of bathymetry at the receiver was changed from 127 to 128 m in order to correspond better with the estimate of Ref. 1. The change in the sediment thickness was based on subbottom profiling measurements conducted near the vertical array location.[29] A range-independent baseline environmental model was constructed using only the receiver bathymetry and sound-speed profile. Table I summarizes the parameter values selected for the baseline environmental model. In Table I the receiver depth is the depth of the hydrophone closest to the ocean bottom; this parameter controls the depth of all of the hydrophones. The following notation is used for the sound-speed profile in the sediment, c_0, c_5, c_{20}, and c_{50}, where the subscript denotes the depth of the profile point below the ocean sediment interface and c_b denotes the sound speed in the bottom.

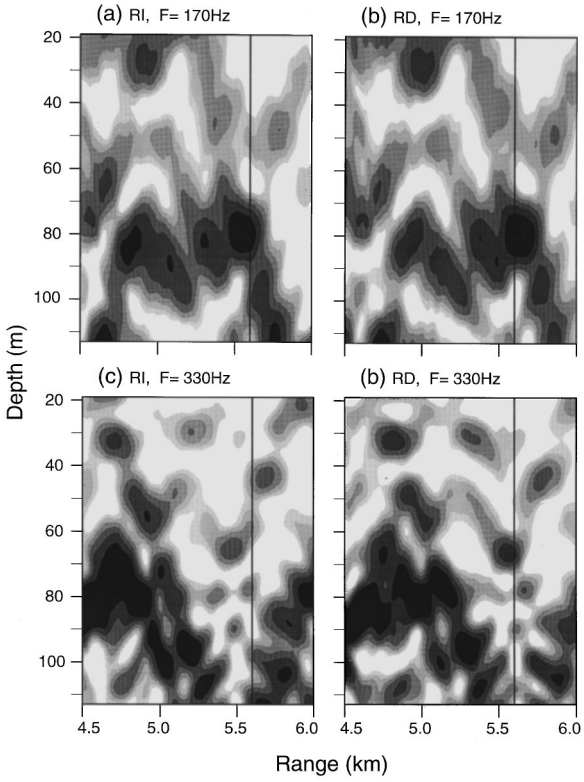

FIG. 4. Contour plots of the transmission loss for range-independent (RI) and range-dependent (RD) environment at 170 and 330 Hz; (a) RI at 170 Hz, (b) RD at 170 Hz, (c) RI at 330 Hz, and (d) RD at 330 Hz. The vertical line is at 5.6 km, the dynamic range of the contours is 10 dB.

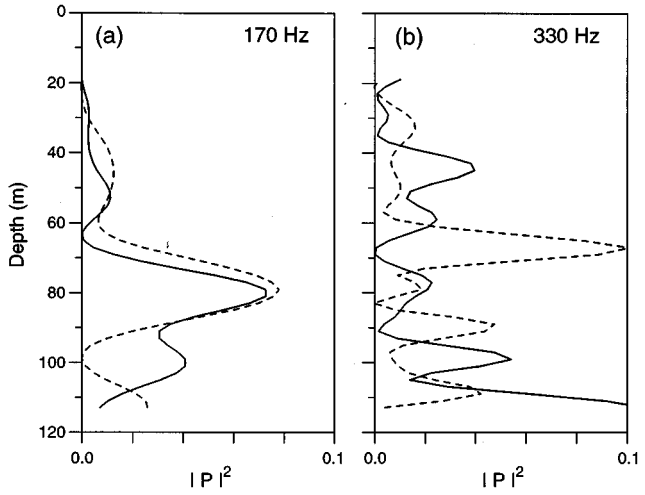

FIG. 5. Magnitude squared of the predicted pressure, at 5.6 km, using the baseline models, range-independent model (solid line), range-dependent model (dashed line); (a) 170 Hz and (b) 330 Hz.

The range-dependent and range-independent baseline models were used to provide an acoustic description of the environment. The SACLANTCEN normal mode propagation model, (SNAP),[30] was used to compute transmission loss as a function of depth and range for both baseline models at 170 and 330 Hz, see Fig. 4. By taking a cut at a range of 5.6 km the magnitude squared of the normalized pressure as a function of depth over the array aperture for both baseline models at 170 and 330 Hz was obtained, see Fig. 5. For the 170-Hz signal, Fig. 5(a), it is seen that the predicted pressures for the two models are fairly similar. For the 330-Hz signal, Fig. 5(b), it is seen that the impact of the range dependence is substantial. The two predicted pressures are not similar at any depth. The influence of the range dependence of bathymetry and ocean sound speed is significant at the higher frequency.

By comparing the transmission loss contour plots for the range-independent and the range-dependent environments, see Fig. 4, for each frequency the impact of the range dependence can be understood. It is seen that the range dependence causes a stretching of the field in range, at 5.6 km this stretching is about 100 m. A major part of the stretching is due to the larger average bathymetry for the range-dependent model. The amount of stretching depends on each mode and its interaction with the seabottom. The 330-Hz field is varying so fast with range that a 100-m offset causes the field to

TABLE III. The GA parameter estimates using a range-independent (RI) and a range-dependent (RD) inversion model, estimates are GA-best. The synthetic data have been generated by the RD baseline environment.

Model parameter	Baseline	GA-RI 170 Hz	GA-RI 330 Hz	GA-RD 170 Hz	GA-RD 330 Hz
Bartlett power (dB)		−0.06	−0.64	−0.02	−0.05
Geometric					
Source range (m)	5600	5550	5512	5602	5611
Source depth (m)	80.0	80.5	79.3	80.0	80.2
Receiver depth (m)	112.7	114.0	112.5	113.3	111.2
Array tilt (m)	0	−0.07	0.6	−0.07	0.26
Bathymetry-src (m)	130	129.5	128.7	130.5	130.7
Bathymetry-rcv (m)	128	⋯	⋯	128.5	127.6
Sediment					
Sound speed, c_0 (m/s)	1520	1516	1511	1518	1521
Sound speed, c_5 (m/s)	1550	1556	1566	1562	1551
Sound speed, c_{20} (m/s)	1600	1656	1566	1587	1583
Sound speed, c_{50} (m/s)	1650	1716	1624	1653	1599
Attenuation (dB/λ)	0.13	0.19	0.18	0.20	0.12
Bottom					
Sound speed, c_b (m/s)	1750	1889	1777	1669	1690

appear significantly different on the array, Fig. 5(b), whereas at 170 Hz the influence is less significant.

III. SYNTHETIC DATA INVERSIONS

In this section it will be shown that the inversion results based on the synthetic data in the 170-Hz band are not sensitive to the mildly range-dependent environment, whereas the inversion results based on 330-Hz band data are sensitive. The analysis is concentrated on one frequency for each band. The range-dependent baseline environmental model, see Table I, was used to generate a synthetic data vector for the 48-sensor array at 170 and 330 Hz. These data were used as input to the GA to determine the estimation performance as a function of frequency and range dependence. The GA search parameters were: population size 64, reproduction size 0.5, cross-over probability 0.8, mutation probability 0.05, number of iterations 2000 and number of independent populations 10. The inversion model and the parameter search bounds used are summarized by Table II. For those parameters which were not optimized the baseline values of Table I were used. The sediment and bottom sound speeds were linked together using shape functions, see Eq. (7). For this case the shape functions were

$$c_5 = c_0 + \delta_1\,, \quad c_{20} = c_5 + \delta_2\,,$$
$$c_{50} = c_{20} + \delta_3\,, \quad c_b = c_{50} + \delta_4\,. \tag{8}$$

The GA optimization was carried out over the four shape coefficients δ_j, $j=1,...,4$, between the bounds indicated in Table II.

The inversion model, see Table II, was used by the GA for both a range-independent and range-dependent inversion. The results for both inversions (range-independent and range-dependent) are provided in Table III. Examining the results summarized in Table III the first issue to notice is the Bartlett power. For the range-independent inversion the Bar-

TABLE IV. The models used for inversion. The notation (n) denotes that there are n values used for that parameter. For bathymetry this refers to the source and receiver bathymetry. sr denotes source range, sd denotes source depth, rd denotes receiver depth, cp denotes sound-speed points in the water. N_{RI} and N_{RD} is the number of parameters over which optimization was performed for range-independent and range-dependent environments, respectively.

Model	N_{RI}	N_{RD}	Inversion parameters
1	2	2	sr, sd
2	3	4	sr, sd, bathy.(2)
3	4	5	sr, sd, bathy.(2), tilt
4	8	9	sr, sd, bathy.(2), tilt, $c_{0,5,20,50}$
5	11	12	sr, sd, bathy.(2), tilt, $c_{0,5,20,50}$, rd, c_b, sed.att.
6	⋯	18	sr, sd, bathy.(2), tilt, rd, $c_{0,5,20,50}$ (2), sed.att. (2), c_b (2)
7	16	⋯	sr, sd, bathy., tilt, $c_{0,5,20,50}$, rd, c_b, sed.att. EOF(5)
8	32	⋯	sr, sd, bathy., tilt, $c_{0,5,20,50}$, rd, c_b, sed.att. cp(21)

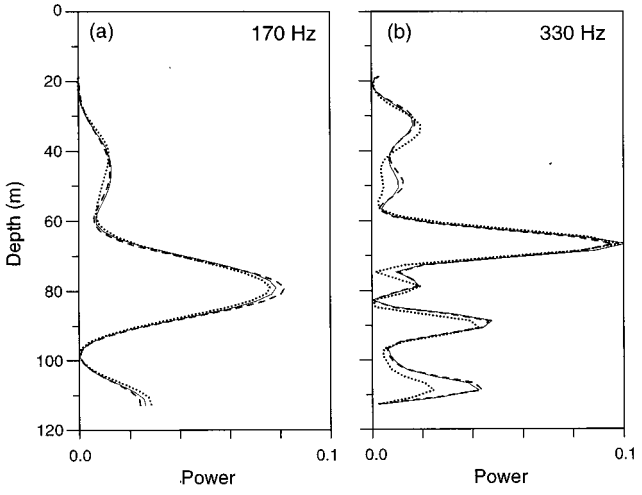

FIG. 6. Magnitude squared of the synthetic pressure using the range-dependent baseline environmental model (solid line), the Bartlett power versus depth measure resulting from the estimated parameters GA-RD (dashed line) and GA-RI (dotted line); (a) 170 Hz and (b) 330 Hz.

TABLE V. GA-best Bartlett power and source location estimates for each inversion model of Table IV, both range independent (RI) and range dependent (RD).

	170-Hz band			335-Hz band			Both bands		
Model	Power (dB)	Range (m)	Depth (m)	Power (dB)	Range (m)	Depth (m)	Power (dB)	Range (m)	Depth (m)
RI-1	−0.40	5450	75	−4.70	5300	74	−2.93	5470	75
RI-2	−0.31	5500	76	−1.81	5610	78	−1.21	5590	78
RI-3	−0.29	5490	76	−1.65	5580	78	−1.16	5570	77
RI-4	−0.24	5490	76	−1.50	5620	77	−1.09	5560	77
RI-5	−0.24	5500	75	−1.04	5640	78	−0.92	5590	77
RD-1	−0.41	5560	76	−2.59	5320	76	−2.12	5580	77
RD-2	−0.28	5610	75	−1.04	5670	80	−0.76	5660	80
RD-3	−0.25	5590	75	−0.96	5650	80	−0.71	5650	79
RD-4	−0.22	5600	75	−0.95	5670	79	−0.68	5630	79
RD-5	−0.22	5600	76	−0.98	5630	78	−0.65	5660	80
RD-6	−0.23	5560	77	−0.75	5650	80	−0.60	5630	79

tlett power is significantly degraded at 330 Hz, whereas for the range-dependent inversion, at both frequencies, the Bartlett power is close to the maximum, i.e., 0 dB. Thus as previously noticed in Fig. 5(a) and (b), the impact of the range dependence is more significant at the higher frequency. The source range estimates improved considerably with the range-dependent inversion. Of course the bathymetry estimates are improved with the range-dependent inversion. The estimates of compressional speed for the sediment were also improved by use of the range-dependent inversion.

Figure 6 illustrates the magnitude squared of the synthetic data vector (solid line) as a function of depth over the array aperture, the Bartlett power versus depth measure (dashed line) based on the GA-RD estimated parameters and the Bartlett power versus depth measure (dotted line) based on the GA-RI estimated parameters. It is seen that, at both frequencies, the fit between the magnitude squared of the data vector and the Bartlett power measure is quite good for the GA-RD estimated parameters, whereas for the GA-RI parameters the fit is good at 170 Hz but not at 330 Hz. This figure, together with the parameter estimates in Table IV discussed above, illustrates the advantages of using the range-dependent inversion at the higher frequency.

These simulations indicate that if the actual environment at the North Elba site is fairly close to the baseline environmental model the range-dependent inversion model should work quite well for estimating the geometric and geoacoustic parameters at both frequencies. In addition, these simulation results support the previous results of Ref. 1 that a range-independent model performs well at 170 Hz for this environment.

IV. INVERSION OF MULTIFREQUENCY DATA

A baseline environmental model for the North Elba site was presented in Fig. 3 and Table I. The objective of the analysis in this section is to refine this baseline environmental model by inversion of the acoustic field data using GA. An issue addressed is the determination of the ''best'' inversion model, that is, which of the entire set of environmental parameters were important to the GA optimization. This issue is dealt with by performing the inversion using a number of inversion models. The estimation performance as a function of frequency is also addressed.

Since the two PRN signals were not transmitted simultaneously two time segments were used in the analysis. The first segment (170-Hz signal) was collected at 15:13, the second segment (335-Hz signal) was collected at 15:54. Since all parameters, except for array tilt (which was known to be small), could be considered stationary, the fact that different time periods were used was not considered an issue. The frequency domain data vector $\mathbf{q}(\omega)$ for the 48 hydrophones was formed using 4096 time samples sampled at a sample rate of 1 kHz. For each frequency a cross-spectral matrix was computed as the outer product of the observation vectors, $\mathbf{q}(\omega)\mathbf{q}^*(\omega)$, normalized by the norm of the observation vector squared. An average over two time epochs was computed, thus each matrix represented a total time sample of approximately 8 s. The bands from 165 to 175 Hz and 325 to 335 Hz were processed and for each band 3 frequencies with a large power were selected (at approximately 0.25, 0.5, and 0.75 times the 10-Hz frequency band). The selected frequencies were 167.7, 169.2, 172.6, 327.6, 330.1, and 332.5 Hz.

The selection of these frequencies was somewhat arbitrary, and other schemes could have been used. Ideally, to obtain more robust estimates the inversion should be based on data from frequencies spaced further apart. However, as is evident from Figs. 1 and 2 there is different information available at each of the selected frequencies and during preliminary inversion runs it was found that data from two or

TABLE VI. Standard deviations (normalized by the search interval) calculated using the *a posteriori* distributions for the geometric parameter estimates for model RD-6.

Parameter	170-Hz band	335-Hz band	Both bands
Source range	0.03	0.03	0.03
Source depth	0.08	0.08	0.05
Receiver depth	0.27	0.28	0.22
Array tilt	0.04	0.04	0.02
Bathymetry-src	0.13	0.09	0.07
Bathymetry-rcv	0.13	0.17	0.13
Mean	0.11	0.11	0.09

more frequencies should be used in each band. However, the environmental information that can be extracted does not vary within a band as the wavelength is nearly constant in each band. Basing the estimate of the covariance matrix on longer observation times was not found important.

A major concern for a global approach is the CPU time. Nearly all CPU time is used generating the forward model results (here 20 000 times). These CPU times are reported for a DEC 3000/800 workstation. At one end of the scale the inversion for the three frequencies in the 170 Hz band for the range-independent model took 40 min and at the other end of the scale it took 5 h for the range-dependent inversion using all six frequencies for the combined band.

Throughout this section the estimation results are based on use of the incoherent frequency averaged Bartlett processor, see Eq. (1), as the objective function. The GA search parameters, e.g., population size, reproduction size, etc., were the same as those used in Sec. III, see Table III for the optimization search bounds.

A. The inversion models

In order to investigate the issue of parameter importance a number of inversion models of increasing complexity were constructed, see Table V. Model 1 provided optimization over only the source location parameters, whereas model 2 added optimization over the bathymetry. Model 5 is the same as that used in the simulations of Sec. III. Model 6 was the most complex with optimization over geometric parameters as well as sediment and bottom parameters for a range-dependent environment. Models 7 and 8 are used with the range-independent model to optimize over ocean sound speed. Model 7 uses EOFs while model 8 uses individual sound-speed points. The results of models 7 and 8 are discussed in Sec. IV D.

An inversion was computed using the incoherently averaged Bartlett processor for all models of Table V. The data were processed using three different bands; (a) incoherent average over the three frequencies from the 170-Hz band, (b) incoherent average over the three frequencies from the 335-Hz band, and (c) incoherent average over the six frequencies from both bands. A summary of the inversion results in terms of Bartlett power and source location parameters is given in Table VI.

In commenting on this table it should be made clear that Monte-Carlo global optimization methods are good at finding a solution close to the global optimum, but not *the* best value. How close it gets to the global optimum depends on the actual problem and the GA-tuning parameters, especially the number of forward modeling runs. When using only 20 000 forward runs for each inversion the search has not yet been exhausted and the error is estimated to about 5% of the Bartlett power. Some of this uncertainty could be reduced by combining the global search with a deterministic search algorithm.[6] The number of forward runs and this uncertainty will also influence the *a posteriori* distributions. By increasing the number of forward modeling runs the peaks in the *a posteriori* distributions become sharper.

Examining the results of Table VI it is seen that many of the issues observed in the synthetic data results, presented in Table III of Sec. III, are the same. That is, the Bartlett power is larger for the 170-Hz band than for the 335-Hz band and that the Bartlett power for the 335-Hz band increased with a range-dependent model. Using the results of Table VI, which contains 5 range-independent models, 6 range-dependent models each for the three frequency bands the assessment of global estimation performance as a function of frequency, as a function of range dependence and as a function of model complexity is addressed. The two range-independent models containing optimization over ocean sound speed are discussed in Sec. IV D.

B. Inversion performance

For the 170-Hz band the Bartlett power is essentially flat as a function of model complexity beyond models RI-4 and RD-3, indicating that at 170 Hz the estimation was not sensitive to additional environmental complexity. If only the 170-Hz band data were available the simplest model to use, based on Bartlett power, would be the range-independent model RI-4. Examining the results for the other bands it is seen that the higher frequency data, 335-Hz band and combined band, appear to support a larger number of model parameters since the Bartlett power continues to improve as the models become more complex. Due to the fact that there are more modes propagating at 335 Hz there is more information at the higher frequencies. Therefore, there may be a gain by using a more complicated model at the higher frequency.

Since the baseline values for source range and depth were not known exactly it was not possible to determine which band provided the most accurate source location estimates. [Based on measurements, the source range and depth were estimated to 5600 ± 200 and 80 ± 2 m (Ref. 1).] The *a posteriori* distributions provided some insight. Figure 7 illustrates the *a posteriori* distributions for source range and depth for each of the three bands using model RD-6 for comparison. Examining Fig. 7 it is seen that the source range and depth distribution becomes more compact when the combined band is used instead of the individual bands. It can also be seen that the 170-Hz band gives lower estimates for range and depth than the 335-Hz band. The source range and depth estimates of the combined band are mainly influenced by the higher frequency data. These results indicate that the objective function is less ambiguous for the combined band, and thus more reliable source location parameter estimates are obtained using the combined band.

Further insight was gained by examining the empirical standard deviations (normalized by the search interval) calculated from the *a posteriori* distributions. Table VII provides the normalized standard deviations for each of the geometric parameter estimates obtained using model RD-6. The estimates obtained using the combined band are more stable than those obtained using either of the two other bands and the mean standard deviation is smaller. For all of the parameters, geometric, and geoacoustic (not shown), the combined band provided the most stable, or was equal to the most stable, estimate. In summary, the stability of the parameter estimates for the combined band would indicate that it should be used.

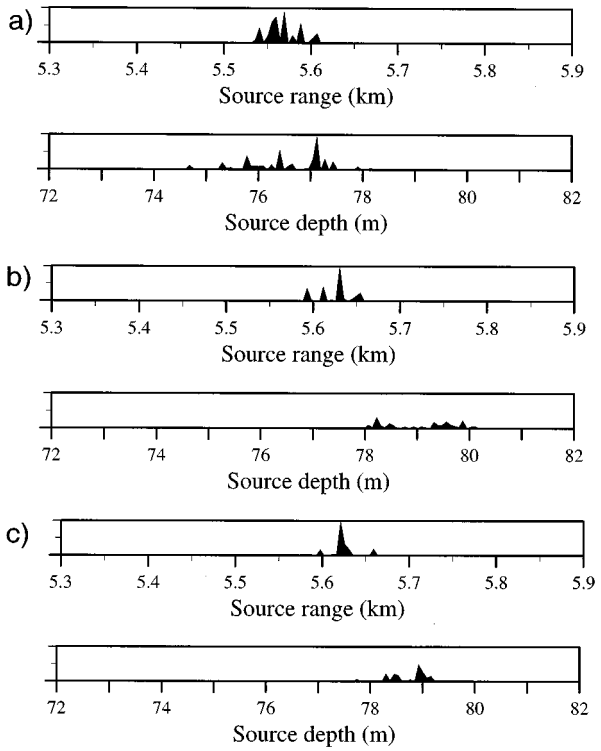

FIG. 7. The *a posteriori* distributions for source range and depth for model RD-6; (a) 170-Hz band, (b) 335-Hz band, and (c) the combined bands.

Returning to Table VI it is seen that, as for the synthetic results (Table III), the use of a range-dependent model was advantageous. That is, the Bartlett power for all models increased with the range-dependent model. It should also be noted that the range and depth estimates for the range-dependent models were quite stable and close to the baseline values.

C. Performance of the RD-6 model

Using the Bartlett power as a performance measure it is seen from Table VI that the model with the largest Bartlett power is the range-dependent model RD-6 when the combined band is used. Even though the largest Bartlett power was obtained using the RD-6 model it may be over interpretation to use all the parameters of that model; for example RD-4 might be sufficient, as the improvement in Bartlett power is not large between the two models. This implies that the most uncertain parameters for model RD-6 should be interpreted with care.

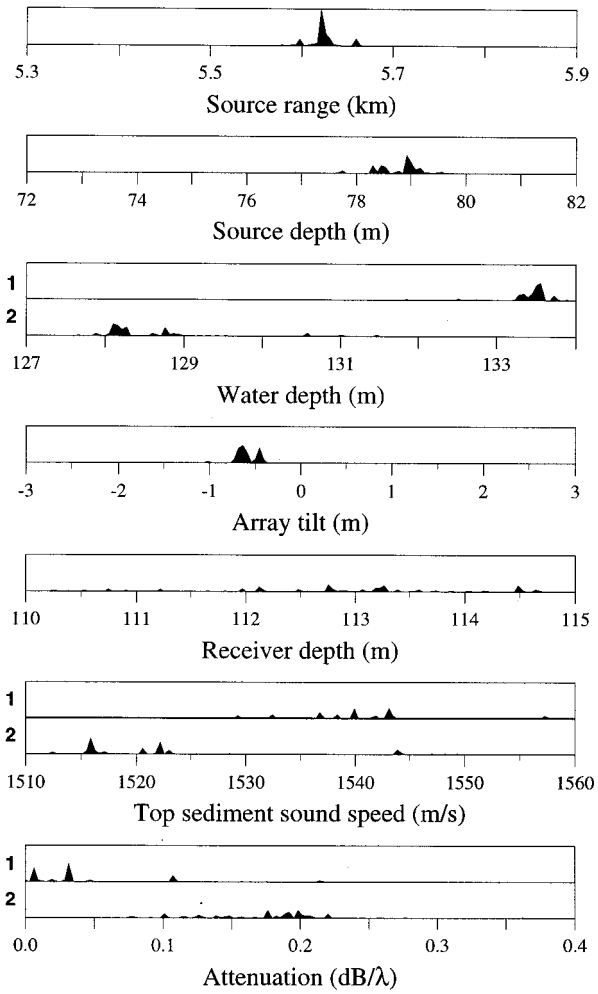

FIG. 8. The *a posteriori* distribution for the most important parameters for model RD-6 using the combined band. 1 and 2 refers to the source and receiver environment, respectively.

For the RD-6 model the *a posteriori* distributions for the more important parameters are illustrated in Fig. 8. It is seen that except for the receiver depth the geometric parameters were well determined. That is, all distributions were compact over the search interval and had well defined single peaks. In general, it would be expected that the source and receiver depths are about equally important. The source depth is much more important here because it is placed in the thermocline. Further, the search interval for the receiver depth is half of the search interval for the source depth. For the sediment sound-speed estimates a plot of the GA-best value of

TABLE VII. GA-best and GA-mean Bartlett power and source location estimates for the inversion model of RI-7 and RI-8 in Table IV.

	170-Hz band			335-Hz band			Both bands		
Model	Power (dB)	Range (m)	Depth (m)	Power (dB)	Range (m)	Depth (m)	Power (dB)	Range (m)	Depth (m)
GA-best RI-7	−0.27	5780	77	−0.68	5310	78	−0.71	5450	76
GA-best RI-8	−0.22	5700	77	−0.41	5540	76	−0.63	5660	78
GA-mean RI-7	−0.26	5720	77	−0.79	5400	75	−0.71	5560	77
GA-mean RI-8	−0.23	5670	77	−0.51	5470	76	−0.51	5720	77

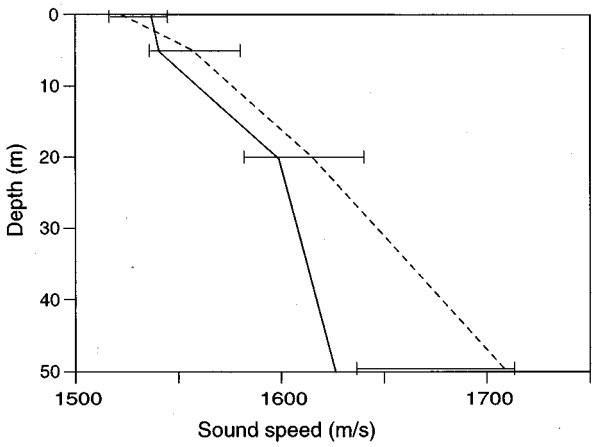

FIG. 9. The GA-best estimate of sediment sound speeds using model RD-6 at the source (solid line) and at the receiver (dashed line). The horizontal bars indicates one standard deviation to either side of the mean of the *a posteriori* distribution.

the *a posteriori* distribution for the two profiles is included as Fig. 9. From the *a posteriori* distribution the standard deviation for each sound-speed point has been estimated and is included as error bars in the figure. It is seen that the standard deviation increases with depth. The lower depths are only determined with considerable uncertainty (i.e., large standard deviations), as the sound speed at these depths is not important for the wave propagation in the water column. In general only the first few wavelengths (corresponding to 20–30 m) of the sediment are important for the wave propagation.

In order to better understand the performance of the GA environmental parameter estimates at each of the six frequencies the Bartlett power measure for model RD-1 and RD-6 is plotted in Fig. 10. The solid line represents the magnitude-squared pressure across the array, Eq. (5), and the dashed line and dotted line represent Bartlett power measure, Eq. (6), for the best environment for model RD-1 and RD-6, respectively. The closer the two lines are the better the fit between the model and the data. From the figure it is seen that, as noted earlier, the optimization over environmental parameters is mainly improving the fit at the higher frequencies, RD-6 provides a better fit than RD-1.

D. Ocean sound speed

During the conduct of the experiment 15 CTD's were collected (a CTD is a probe for measuring conductivity temperature and density in the ocean). The sound-speed variability was small, less than ± 1 m/s, for the corresponding sound-speed profiles. These sound-speed profiles formed a data base for calculating the EOFs. Through an empirical procedure minimizing the error between the series representation, Eq. (A3), and the actual sound-speed profiles it was determined that five EOFs were sufficient.

As described in Sec. I C, three representations of the sound-speed profile are available, individual sound-speed points (model RI-8), EOFs (model RI-7) and *ad hoc*. The *''ad-hoc''* sound-speed representation is not described since sufficient sound-speed observations were available and thus

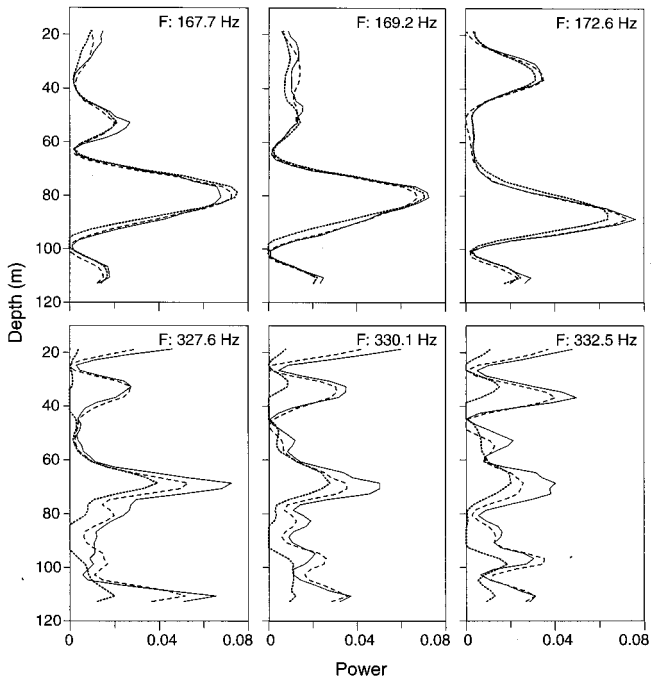

FIG. 10. The power across the array for each of the six frequencies. Magnitude squared of the pressure (solid line), Bartlett power measure, Eq. (3), for RD-1 estimates (dotted line), and for RD-6 estimates (dashed line).

EOFs were preferable. For the EOF coefficients (model RI-7) the search interval was -5 to 5 m/s for the five coefficients, thus in total 16 parameters were used in this optimization. For the individual sound-speed points (mode RI-8), 21 points were used in describing the profile, and each point was given a search interval of -2 to 2 m/s around the mean profile.

The results of both inversions are given in Table IV and the corresponding sound-speed profiles in Fig. 11. The results obtained for RI-8 are unusual, as it has too many free variables. This causes a very good fit, but the model should be rejected because it has an unphysical sound-speed profile. As the GA-mean does not represent an actual sampled model vector it is possible that the GA-mean Bartlett power is better that the GA-best, as is the case for the combined band of RI-8. It is seen that RI-7 has a better fitness than the other range-independent models, but the estimated range is further away from the baseline value.

The estimated sound-speed profiles are shown in Fig. 11 using models: (a) RI-8 and (b) RI-7. The sound-speed measurements taken at the source and receiver are shown for reference. From the *a posteriori* distribution the standard deviation for some of the sound-speed points have been estimated and are included as error bars in the figure. The standard deviations indicate that sound-speed estimation based on the individual sound-speed points is more uncertain. The estimated sound-speed profiles are based on the mean of the *a posteriori* distribution as the individual sound-speed points gave an unrealistic profile when the GA-best estimate was used. The use of the GA-mean works as a regularization tool that smooths out the unrealistic high frequency variations in the profile. The lower part of the profile is smoother than the

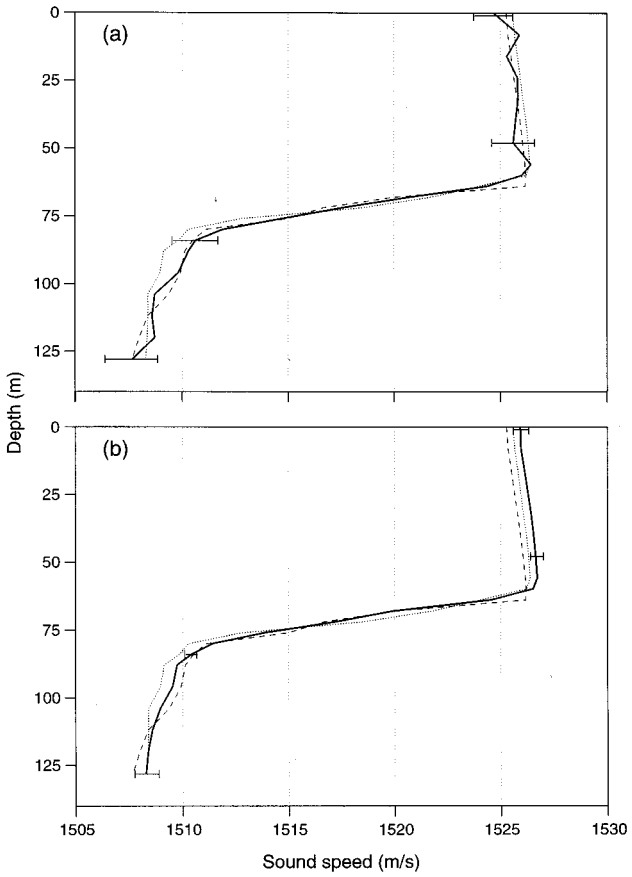

FIG. 11. Estimated GA-mean ocean sound-speed profiles (solid line) using: (a) RI-8 (sound-speed points) and (b) RI-7 (EOFs). For reference, the sound-speed profile at the receiver (dashed line) and at the source (dotted line) are shown. The horizontal bars indicate one standard deviation to either side of the GA-mean.

upper which could indicate that it is more well determined, probably because the lower part is more important for the wave propagation. The extra degrees of freedom for the sound speed enables it to obtain a good Bartlett power. In fact, this is the best Bartlett power for all range-independent models. This underlines how important the ocean sound-speed profile is for the wave propagation, and thus the estimated parameters. If there are minor uncertainties in the ocean sound speed this can have a major influence on the estimates of the remaining parameters. In order to obtain a physically realistic estimate using single sound speed points the solution has probably to be regularized so that either the deviation from an expected profile is penalized or the second derivative of the profile is penalized.[31]

The estimated sound-speed profile using EOFs is close to the expected, and also the estimated values for the geometric and geoacoustic parameters are close to those found without optimizing over ocean sound speed.

V. CONCLUSIONS

Inversion was performed using high-quality acoustic field data collected on a vertical array in a mildly range-dependent shallow water environment. Two signal bands were used, a band centered around 170 Hz and a band centered around 335 Hz. Inversion at a single frequency, 169.9 Hz, using this data has previously been reported.[1]

Data from several frequencies were combined using the incoherent Bartlett processor. When the inversion was based on several frequencies it was found that the solution became more stable. The lower frequency data were easier to invert since there are fewer modes and thus less information about the environment in the observations. At the higher frequency more parameters can be estimated as there are more modes and thus more information.

A range-dependent adiabatic normal mode code was used for the forward model. The lower frequency data did not require range dependence, but the Bartlett power for the higher frequencies improved significantly when range dependence was included. With the range-dependent model (RD-6) a Bartlett power of -0.6 dB (compared to 0 dB maximum) was obtained using the combined frequency band, clearly indicating that a good environmental model was found.

Inclusion of the ocean sound speed in the inversion process was also investigated for a range-independent environment. As acoustic data is very sensitive to the ocean sound speed it should in general be included. The sound speed was represented using both individual sound-speed points as well as empirical orthonormal functions (EOFs). In the present case a Bartlett power of -0.6 dB was obtained when using EOFs, indicating that also this environmental model could be likely.

The global estimation method, genetic algorithms, was applied to experimental observations at several frequencies for estimating the geometric, geoacoustic, and ocean sound-speed model parameters. The geometric parameters such as source range and depth, array hydrophone positions, and bathymetry were included in the search. Thus all important forward model parameters in a range-dependent environment using acoustic field observations were estimated. Based on the *a posteriori* distributions the geometric parameters were well estimated and the resolution of the first few wavelengths of the bottom is probably sufficient for most underwater acoustic applications.

APPENDIX: EMPIRICAL ORTHONORMAL FUNCTIONS

The use of empirical orthonormal functions (EOF) for representing ocean sound-speed profiles follows directly from the Karhunen–Loeve expansion from random process theory.[32] The method is straightforward, given a sequence of sound-speed vectors $\{\mathbf{c}^m\}$ $m=1,2,\ldots,M$, sampled at D discrete points $\{z_1,z_2,\ldots,z_D\}$. First form a sample mean vector $\overline{\mathbf{c}}$. A set of orthonormal vectors $\mathbf{v}_j$, the EOFs or shape functions, are determined as the eigenvectors of the sample covariance matrix $\mathbf{C}$ given by

$$\mathbf{C}=(1/M)\sum_{m=1}^{M}(\mathbf{c}^m-\overline{\mathbf{c}})(\mathbf{c}^m-\overline{\mathbf{c}})^T. \tag{A1}$$

The orthonormal vectors could also be found by ordering all the observed sound-speed vectors into a single matrix $\mathbf{Q}=[\mathbf{c}^1-\overline{\mathbf{c}},\mathbf{c}^2-\overline{\mathbf{c}},\ldots,\mathbf{c}^M-\overline{\mathbf{c}}]$ and then do a singular value decomposition of this matrix, i.e., $\mathbf{Q}=\Sigma_{j=1}^{M}\lambda_j\mathbf{v}_j\mathbf{u}_j^T$. The cova-

riance matrix $\mathbf{C}$ can then be expressed in terms of the singular eigenvectors:

$$\mathbf{C}=\mathbf{Q}\mathbf{Q}^T=\sum_{j=1}^{M}\lambda_j^2\mathbf{v}_j\mathbf{v}_j^T\,. \tag{A2}$$

Thus the eigenvectors of the covariance matrix Eq. (A1) and the singular vectors $\mathbf{v}_j$ are identical. They are, though, arrived at from different viewpoints.

For any one of the sound-speed vectors a series representation, using J terms, is given by [similar to Eq. (7)]

$$(\mathbf{c}-\overline{\mathbf{c}})=\sum_{j=1}^{J}\mu_j\mathbf{v}_j\,, \tag{A3}$$

where the coefficients μ_j are given by the vector inner product

$$\mu_j=(\mathbf{c}-\overline{\mathbf{c}})^T\mathbf{v}_j\,. \tag{A4}$$

The global optimization for ocean sound-speed estimation is carried out over the EOF coefficients $\{\mu_j\}$ where the number of coefficients J is selected based on experience.

[1] D. F. Gingras and P. Gerstoft, ''Inversion for geometric and geoacoustic parameters in shallow water: Experimental results,'' J. Acoust. Soc. Am. **97**, 3589–3598 (1995).

[2] M. D. Collins, W. A. Kuperman, and H. Schmidt, ''Nonlinear inversion for ocean-bottom properties,'' J. Acoust. Soc. Am. **92**, 2770–2783 (1992).

[3] C. E. Lindsay and N. R. Chapman, ''Matched field inversion for geophysical parameters using adaptive simulated annealing,'' IEEE J. Ocean. Eng. **OE-18**, 224–231 (1993).

[4] S. E. Dosso, M. L. Yeremy, J. M. Ozard, and N. R. Chapman, ''Estimation of ocean bottom properties by matched field inversion of acoustic field data,'' IEEE J. Ocean. Eng. **OE-18**, 232–239 (1993).

[5] P. Gerstoft, ''Inversion of seismoacoustic data using genetic algorithms and *a posteriori* probability distributions,'' J. Acoust. Soc. Am. **95**, 770–782 (1994).

[6] P. Gerstoft, ''Inversion of acoustic data using a combination of genetic algorithms and the Gauss–Newton approach,'' J. Acoust. Soc. Am. **97**, 2181–2190 (1995).

[7] P. Gerstoft, ''SAGA: Seismo-Acoustic inversion using Genetic Algorithms,'' unpublished SACLANTCEN document, 1995.

[8] A. B. Baggeroer, W. A. Kuperman, and H. Schmidt, ''Matched field processing: Source localization in correlated noise as an optimum parameter estimation problem,'' J. Acoust. Soc. Am. **83**, 571–587 (1988).

[9] E. K. Westwood, ''Broadband matched-field source localization,'' J. Acoust. Soc. Am. **91**, 2777–2789 (1992).

[10] P. Mignerey and S. Finette, ''Multichannel deconvolution of an acoustic transient in an oceanic waveguide,'' J. Acoust Soc. Am. **92**, 351–364 (1992).

[11] D. F. Gingras, ''Robust broadband matched-field processing: Performance in shallow water,'' IEEE J. Ocean. Eng. **OE-18**, 253–264 (1993).

[12] T. C. Yang, ''Broadband source localization and signature estimation,'' J. Acoust. Soc. Am. **93**, 1797–1806 (1993).

[13] I-Tai Lu, H. Y. Chen, and P. Voltz, ''A matched mode processing technique for localizing a transient source in the time domain,'' J. Acoust. Soc. Am. **93**, 1365–1373 (1993).

[14] J-P. Hermand and W. I. Roderick, ''Acoustic model-based matched filter processing for fading time-dispersive ocean channels: Theory and experiment,'' IEEE J. Ocean. Eng. **OE-18**, 447–465 (1993).

[15] C. Feuillade, D. R. Del Balzo, and M. M. Rowe, ''Environmental mismatch for shallow-water matched-field processing: Geoacoustic parameter variability,'' J. Acoust. Soc. Am. **85**, 2354–2364 (1989).

[16] A. Tolstoy, ''Sensitivity of matched field processing to sound-speed profile mismatch in a deep water Pacific environment,'' J. Acoust. Soc. Am. **85**, 2394–2404 (1989).

[17] D. F. Gingras, ''Methods for predicting the sensitivity of matched-field processors to mismatch,'' J. Acoust. Soc. Am. **86**, 1940–1949 (1989).

[18] D. F. Gingras and N. L. Gerr, ''Minimax robust matched-field processing,'' J. Acoust. Soc. Am. **93**, 2798–2808 (1993).

[19] C. F. Mecklenbräuker and J. F. Böhme, ''F-test in Matched Field Processing: Identifying multimode propagation,'' *Proceedings of the IEEE International Conference on Acoustics, Speech and Signal Processing ICASSP-95*, Detroit, Michigan (IEEE, New York, 1995), Vol. 5, pp. 3123–3126.

[20] J. F. Lynch, S. D. Rajan, and G. V. Frisk, ''A comparison of broadband and modal inversions for bottom geoacoustic properties at a site near Corpus Christi, Texas,'' J. Acoust. Soc. Am. **89**, 648–665 (1991).

[21] W. H. Munk and C. Wunsch, ''Ocean acoustic tomography: a scheme for large scale monitoring,'' Deep Sea Res. **26**, 123–161 (1979).

[22] B. Cornuelle, W. Munk, and P. Worcester, ''Ocean acoustic tomography from ships,'' J. Geophys. Res. **94**, 6232–6250 (1989).

[23] A. Tolstoy, O. Diachok, and L. N. Frazer, ''Acoustic tomography via matched field processing,'' J. Acoust. Soc. Am. **89**, 1119–1127 (1991).

[24] L. R. LeBlanc and F. H. Middleton, ''An underwater acoustic sound velocity data model,'' J. Acoust. Soc. Am. **67**, 2055–2062 (1980).

[25] F. B. Jensen, ''Comparison of transmission loss data for different shallow water areas with theoretical results provided by a three-fluid normal-mode propagation model,'' in *Sound Propagation in Shallow Water*, edited by O. F. Hastrup and O. V. Olesen, CP-14, SACLANT (Undersea Research Centre, La Spezia, Italy, 1974), pp. 79–92.

[26] T. Akal, ''Bathymetry and bottom structure of zones near the island of Elba used for acoustical trials in shallow water,'' TM-162, SACLANT Undersea Research Centre, La Spezia, Italy (1970).

[27] T. Akal, C. Gehin, B. Matteucci, and B. Tonarelli ''Measured and computed physical properties of sediment cores, Island of Elba zone,'' M-82, SACLANT Undersea Research Centre, La Spezia, Italy (1972).

[28] D. F. Gingras, L. Troiano, and R. B. Williams, ''Acoustic array positioning in shallow water,'' SM-283, SACLANT Undersea Research Centre, La Spezia, Italy (1994).

[29] E. Michelozzi, ''Sediments of Capraia Basin,'' unpublished SACLANTCEN document, 1993.

[30] F. B. Jensen and M. C. Ferla, ''SNAP-The SACLANTCEN normal mode acoustic propagation model,'' SACLANT Undersea Research Centre, **SM-121**, La Spezia, Italy (1979).

[31] A. Caiti, T. Akal, and R. D. Stoll, ''Estimation of shear wave velocity in shallow marine sediments,'' IEEE J. Ocean. Eng. **19**, 58–72 (1994).

[32] W. B. Davenport, Jr. and W. L. Root, *An Introduction to the Theory of Random Signals and Noise* (McGraw-Hill, New York, 1958).